AFRL-ML-WP-TR-2001-4099

IMPROVED THERMAL BARRIER COATING SYSTEM BASED ON A CATHODICALLY DEPOSITED ALPHA ALUMINA SUBLAYER

Rabi S. Bhattacharya
UES, Inc.
4401 Dayton-Xenia Road
Dayton, OH 45432-1894

Bhaskar S. Majumdar
New Mexico Tech
Department of Materials Science and Metallurgical Engineering
801 Leroy Place
Socorro, NM 87801-4796

APRIL 2001

FINAL REPORT FOR PERIOD 31 MARCH 2000 – 31 DECEMBER 2000

THIS IS A SMALL BUSINESS INNOVATION RESEARCH (SBIR) PHASE I REPORT

Approved for public release, distribution unlimited.

20010725 074

MATERIALS AND MANUFACTURING DIRECTORATE
AIR FORCE RESEARCH LABORATORY
AIR FORCE MATERIEL COMMAND
WRIGHT-PATTERSON AIR FORCE BASE, OH 45433-7750

NOTICE

WHEN GOVERNMENT DRAWINGS, SPECIFICATIONS, OR OTHER DATA ARE USED FOR ANY PURPOSE OTHER THAN IN CONNECTION WITH A DEFINITELY GOVERNMENT-RELATED PROCUREMENT, THE UNITED STATES GOVERNMENT INCURS NO RESPONSIBILITY OR ANY OBLIGATION WHATSOEVER. THE FACT THAT THE GOVERNMENT MAY HAVE FORMULATED OR IN ANY WAY SUPPLIED THE SAID DRAWINGS, SPECIFICATIONS, OR OTHER DATA, IS NOT TO BE REGARDED BY IMPLICATION OR OTHERWISE IN ANY MANNER CONSTRUED, AS LICENSING THE HOLDER OR ANY OTHER PERSON OR CORPORATION, OR AS CONVEYING ANY RIGHTS OR PERMISSION TO MANUFACTURE, USE, OR SELL ANY PATENTED INVENTION THAT MAY IN ANY WAY BE RELATED THERETO.

THIS REPORT IS RELEASABLE TO THE NATIONAL TECHNICAL INFORMATION SERVICE (NTIS). AT NTIS, IT WILL BE AVAILABLE TO THE GENERAL PUBLIC, INCLUDING FOREIGN NATIONS.

THIS TECHNICAL REPORT HAS BEEN REVIEWED AND IS APPROVED FOR PUBLICATION.

Rollie E. Dutton

ROLLIE E. DUTTON
Metals Branch
Metals, Ceramics & NDE Division

Katherine A. Stevens

KATHERINE A. STEVENS, Chief
Metals Branch
Metals, Ceramics & NDE Division

Gerald J. Petrak

GERALD J. PETRAK, Asst Chief
Metals, Ceramics & NDE Division
Materials and Manufacturing Directorate

IF YOUR ADDRESS HAS CHANGED, IF YOU WISH TO BE REMOVED FROM OUR MAILING LIST, OR IF THE ADDRESSEE IS NO LONGER EMPLOYED BY YOUR ORGANIZATION, PLEASE NOTIFY, AFRL/MLLMP, WRIGHT-PATTERSON AFB OH 45433-7817 TO HELP US MAINTAIN A CURRENT MAILING LIST.

COPIES OF THIS REPORT SHOULD NOT BE RETURNED UNLESS RETURN IS REQUIRED BY SECURITY CONSIDERATIONS, CONTRACTUAL OBLIGATIONS, OR NOTICE ON A SPECIFIC DOCUMENT.

REPORT DOCUMENTATION PAGE

Form Approved
OMB No. 074-0188

Public reporting burden for this collection of information is estimated to average 1 hour per response, including the time for reviewing instructions, searching existing data sources, gathering and maintaining the data needed, and completing and reviewing this collection of information. Send comments regarding this burden estimate or any other aspect of this collection of information, including suggestions for reducing this burden to Washington Headquarters Services, Directorate for Information Operations and Reports, 1215 Jefferson Davis Highway, Suite 1204, Arlington, VA 22202-4302, and to the Office of Management and Budget, Paperwork Reduction Project (0704-0188), Washington, DC 20503

1. AGENCY USE ONLY (Leave blank)	2. REPORT DATE	3. REPORT TYPE AND DATES COVERED
	April 2001	Final Report, 03/31/2000 – 12/31/2000

4. TITLE AND SUBTITLE
IMPROVED THERMAL BARRIER COATING SYSTEM BASED ON A CATHODICALLY DEPOSITED ALPHA ALUMINA SUBLAYER

5. FUNDING NUMBERS
C: F33615-00-C-5516
PE: 65502F
PR: 3005
TA: ML
WU: 0Q

6. AUTHOR(S)
[1]Rabi S. Bhattacharya
[2]Bhaskar S. Majumdar

7. PERFORMING ORGANIZATION NAME(S) AND ADDRESS(ES)

[1]UES, Inc.
4401 Dayton-Xenia Road
Dayton, OH 45432-1894

[2]New Mexico Tech
Department of Materials Science and Metallurgical Engineering
801 Leroy Place
Socorro, NM 87801-4796

8. PERFORMING ORGANIZATION REPORT NUMBER
UES P702

9. SPONSORING / MONITORING AGENCY NAME(S) AND ADDRESS(ES)

MATERIALS AND MANUFACTURING DIRECTORATE
AIR FORCE RESEARCH LABORATORY
AIR FORCE MATERIEL COMMAND
WRIGHT-PATTERSON AIR FORCE BASE, OH 45433-7750
POC: Rollie Dutton, AFRL/MLLM, 937-255-9834

10. SPONSORING / MONITORING AGENCY REPORT NUMBER
AFRL-ML-WP-TR-2001-4099

11. SUPPLEMENTARY NOTES
This is a Small Business Innovation Research (SBIR) Phase I Report.

12a. DISTRIBUTION / AVAILABILITY STATEMENT
Approved for public release, distribution unlimited.

12b. DISTRIBUTION CODE

13. ABSTRACT ***(Maximum 200 Words)***
This report was developed under a SBIR contract for Topic AF00-146. The primary objective of this Phase I research was to evaluate the feasibility of using an alpha alumina sublayer to reduce oxidation damage and improve the life of advanced thermal barrier coatings (TBC). A patented filtered cathodic arc deposition technique was used to deposit a 0.5-μm-thick alumina sublayer at 1000 °C on a Pt-Al bond-coat deposited on a CMSX-4 single crystal. The unique coating method provides droplet-free coatings and high ionization (>80 percent) compared with standard physical vapor deposition (PVD) techniques (<20-percent ionization). An electron beam PVD technique was used to deposit the yttria stabilized zirconia (YSZ) layer on the alumina coating. Thermal cycling tests were conducted on companion samples between 170 and 1150 °C. Excellent TBC life was obtained when the as-prepared Pt-Al bond-coat was grit blasted with alpha alumina prior to deposition of the alumina layer. Although the control grit-blasted sample, without the alumina layer, also exhibited good cyclic life, it indicated larger oxide thickness and more damage accumulation than the alumina-coated sample. Thus, the alumina sublayer is able to improve TBC performance. The primary mechanism of TBC damage was surface rumpling of the bond-coat, likely due to oxidation and nonuniform shrinkage of the bond-coat.

14. SUBJECT TERMS
SBIR Report, filtered cathodic arc, TBC, thermal barrier coating, alumina coating, alpha alumina, physical vapor deposition, oxidation, yttria stabilized zirconia, turbine engine

15. NUMBER OF PAGES
34

16. PRICE CODE

17. SECURITY CLASSIFICATION OF REPORT	18. SECURITY CLASSIFICATION OF THIS PAGE	19. SECURITY CLASSIFICATION OF ABSTRACT	20. LIMITATION OF ABSTRACT
Unclassified	Unclassified	Unclassified	SAR

NSN 7540-01-280-5500

Standard Form 298 (Rev. 2-89)
Prescribed by ANSI Std. Z39-18
298-102

TABLE OF CONTENTS

LIST OF FIGURES

LIST OF TABLES

TABLES **PAGE**

PREFACE

This technical report has been prepared as part of the requirements of the Phase I SBIR Contract No. F33615-00-C-5516 with the Air Force Research Laboratory/MLLM, Wright-Patterson Air Force Base, Ohio. The report covers work conducted during the period 31 March 2000 through 31 December 2000, and constitutes the final report under this contract. The Air Force Project Engineer was Dr. Rollie E. Dutton.

ACKNOWLEDGEMENT

The authors wish to express their appreciation to Dr. Satish Dixit and Mr. Boris Brodkin for technical support for the coating deposition and Ms. Jan Clark for report preparation.

1.0 INTRODUCTION

Thermal Barrier Coatings (TBCs) are used in the hot section of aircraft engine turbines to increase turbine efficiency and to extend the life of metal components.

1.1 ADVANTAGES OF TBCs

The advantages of thermal barrier coatings (TBCs) in hot section turbine components are best illustrated by Figure 1.

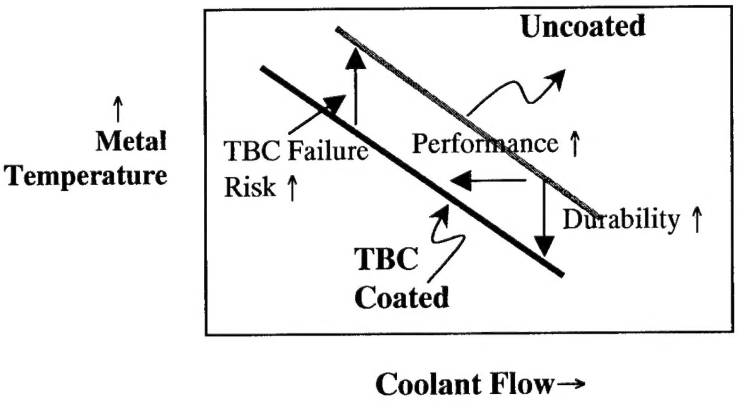

Figure 1. Advantages and risks associated with TBCs.

The main advantages of the TBC are:

(i) At constant coolant flow, they reduce the base metal temperature, thereby increasing the life of that part. Advanced turbine blades in aerospace engines operate very close to their melting temperature, and it is estimated that a 15°C reduction in metal temperature can produce a two-fold increase in life [1-3].

(ii) At existing metal temperature, the temperature at the TBC surface can be increased by as much as 65°C, leading to a substantial gain in fuel efficiency. It is estimated that this temperature advantage is equivalent to two generations of new superalloy development [1-3].

These advantages constitute immense cost savings to the Air Force and the Navy. However, there is a risk factor as well. If the TBC were to delaminate, the increased metal temperature could lead to premature failure of the turbine blade. This is also indicated in Figure 1. The most advanced TBCs to date have matured to provide average life of 500 to 1000 cycles for thermal cycling in the temperature range 200°C to 1150°C[1]. However, reliability and longer life still remain important goals in TBC research, before the benefits of reduced metal temperature are actually implemented in design.

Thus, there is a need to develop TBC systems that have improved reliability and durability than current state-of-the-art systems.

1.2 TBC ARCHITECTURE, MECHANISMS OF FAILURE, & OUR PREVIOUS WORK

We illustrate the four essential components of an advanced TBC system in Figure 2. A platinum aluminide bond-coat is applied to the base superalloy substrate (typically a single crystal), by first

[1] Time at temperature is also an important parameter.

electroplating Pt followed by low activity CVD aluminizing. The thickness of this bond-coat is typically 75-100 μm. Upon this layer is deposited a 6-8 weight percent yttria stabilized zirconia (YSZ) layer of approximately 100 μm thickness. The YSZ is applied by electron beam physical vapor deposition (EB PVD), which provides a columnar structure with high compliance. It is this high compliance that significantly contributes to improved thermal cycling life of advanced TBCs, since it substantially reduces the growth of thermal residual stresses in the YSZ. Between the YSZ and the bond-coat is a thermally grown oxide (TGO) composed mostly of alumina. A very fine TGO may be present before or during deposition of the YSZ, but the majority of the TGO forms during exposure of the TBC system to high temperatures. The growth of the TGO is detrimental to life, since most TBC failures are observed to occur either at the bond-coat/TGO interface, or the TGO/YSZ interface. While the TGO is largely composed of alpha alumina, which is the most stable phase, it can also contain substantial amounts of mixed oxides, such as spinels of the type $Ni(Cr,Al)_2O_4$, or Cr_2O_3, etc. [4-6]. The TGO is a non-equilibrium region, and grows in the presence of oxygen that is continuously fed by the open channel YSZ layer. The typical thickness of TGO after thermal exposure is reported to be about 5 μm [7-9].

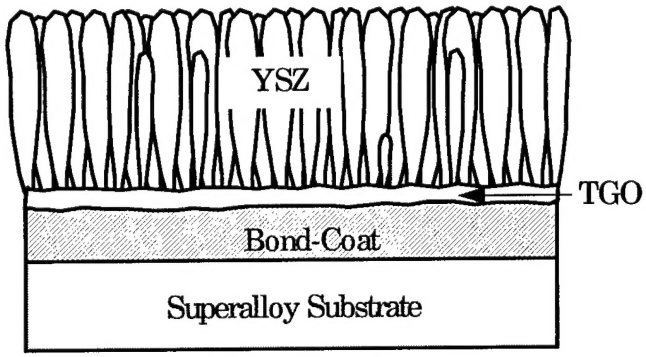

Figure 2. Sketch illustrating the primary components of a traditional thermal barrier coating.

The failure mechanism of the TBC is intimately related to the formation and growth of the TGO. During the initial stages of oxidation, blister type spots can be observed on the TBC surface by thermal wave imaging, or even optically if the blisters are quite large. At a later stage, these blisters either combine, or a single one grows to such a point that a piece of the YSZ layer detaches from the blade. The exact mechanisms and mechanics of failure in the region of the TGO is still a matter of debate. In the case of a flat surface, buckling has been considered to be the predominant mode of final failure of the YSZ layer. However, this mode of failure requires the presence of an initial crack, located either at the bond-coat/TGO interface or at the TGO/YSZ, of approximately 1 to 3 mm length; this length would have been much smaller if the YSZ had the stiffness of dense zirconia. In any case, such calculations indicate that the initial crack in the vicinity of the TGO must increase substantially from a micro-defect before it becomes critical. *The real issue then is what causes growth of initial microdefects at the interface, and how such growth could be eliminated or reduced substantially.*

One postulated source for the microcrack formation and initial growth is heterogeneous volumetric change associated with oxidation of the bond-coat (Figure 3a). This scenario requires volumetric expansion that has yet to be quantified. A second mechanism is the presence of ripples in the TGO (Figure 3b). Figure 4 illustrates results from a finite element method (FEM) analysis with a sinusoidal alumina/YSZ interface [9]. The YSZ layer is on the right, and the TGO is on the left side of the figure. The contour region marked A, at the bond-coat/TGO interface, has an out-of-plane stress (i.e., directed to the right of the figure) of approximately 450 MPa. Thus, fairly large out-of-plane stresses can be generated by interface waviness, enough to nucleate delamination cracks at the interface.

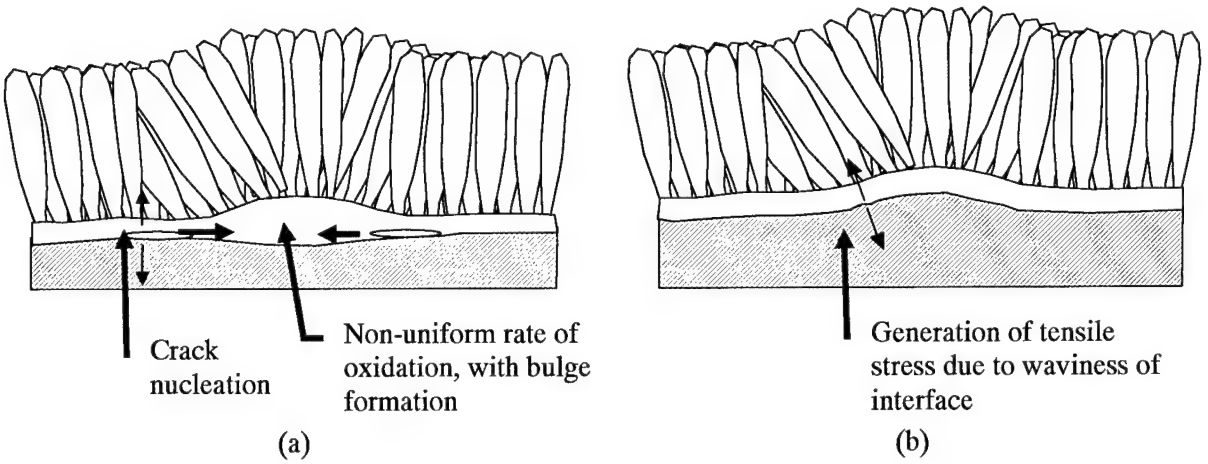

Figure 3. Mechanisms for crack nucleation in the TGO or at the interface. (a) Hetero-geneous oxidation can create a bulge and give rise to normal stresses, thereby nucleating cracks that can then proceed towards the bulge. (b) Non-planar bond-coat deposition or non-uniform oxidation can create surface ripples, which cause generation of out-of-plane tensile stresses.

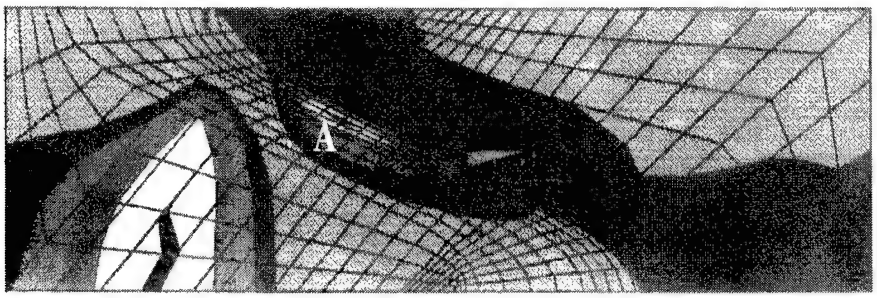

Figure 4. Contour plot from our FEM analysis with a wavy TGO structure. The YSZ layer is on the right, and the bond-coat is on the left. Significant out-of-plane tensile stresses (i.e., along the horizontal axis in the figure) are generated in the small island A (bright) at the bond-coat/TGO interface.

In the case of the diffusion aluminide Pt-Al bond-coat system, large thermal ridges are observed at the grain boundaries of the Pt-modified nickel aluminide (ordered β-NiAl). The ridges (rather than grooves) are a result of outwardly growing aluminide (recall that the Pt layer is electroplated and CVD aluminizing is conducted at the surface). The ridges occupy as much as 10 to 20% of the bond-coat surface (Figure 5), and their heights are in the range 2-5 μm. It is often suggested that these ridges are the cause of delamination initiation and growth until buckling takes over at a crack length of about 2 mm. The problem with this simple viewpoint is that stresses that are normal to the surface will be present right from the start of thermal cycling, and should not depend significantly on the growth of the TGO. Thus, damage should be observable fairly early in the life of the coating. On the other hand, most studies indicate initiation and propagation of damage after some reasonable growth of the TGO layer, typically 2 to 4 μm.

Our previous study on an alumina sublayer based TBC system provided some interesting insight [10]. Figure 6 illustrates a MarM247 alloy with a NiCoCrAlY bond-coat, on which a layer of approximately 0.5 μm thick alumina was deposited using the cathodic deposition technique. The sample was subjected to 1150°C for 100 hours in air, and this appeared to increase the thickness of the alumina

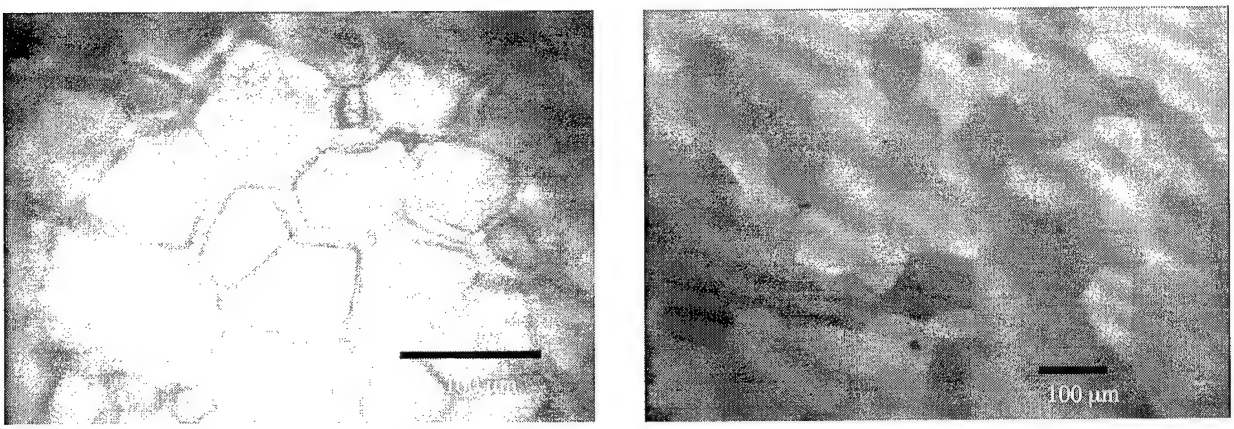

(a) (b)

Figure 5. Surface morphology of a Pt-Al coated single crystal CMSX-4 alloy; (a) as-coated and (b) polished.

to 1-2 μm. The most notable feature was the rumpling of the bond-coat, which appears to have been responsible for spallation of the thin alumina layer. The surface rumpling was accompanied by growth of the bond-coat grains from approximately 3 μm to 25 μm. Also, the Al-rich B2 NiAl grains appeared to be replaced by the Ni and Cr rich fcc gamma phase. The wavelength of the surface rumpling was much larger than any oxide scale thickness, suggesting that the oxide per se was not responsible for the rumpling. The effect of thermal mismatch stress between the bond-coat and the substrate was another possibility. A vacuum treated sample (albeit only for 4 hours at 1150°C) did show slight rumpling, but much less than the oxidized samples. The effect of oxygen ingress through the alumina layer, or through possible cracks in the alumina layer, remained a possibility. This was consistent with changes in the microstructure, wherein the Al rich NiAl phase appeared to be reduced. Overall, the study indicated that microstructural changes (both grain growth and phase modifications), possibly related to oxygen ingress or oxidation at the surface, was a major factor in the formation of rumples and ultimate delamination of the film. Thus, the concept of an alumina sublayer to reduce oxidation was correct, but a more microstructurally stable system was needed for temperatures in the region of 1150°C. In addition, the previous investigation focused only on samples without an outer YSZ layer. A thin layer is more prone to buckling induced delamination failure, as can be deduced from simple buckling analysis. Thus, studies were needed on a more stable bond-coat and with the top YSZ layer.

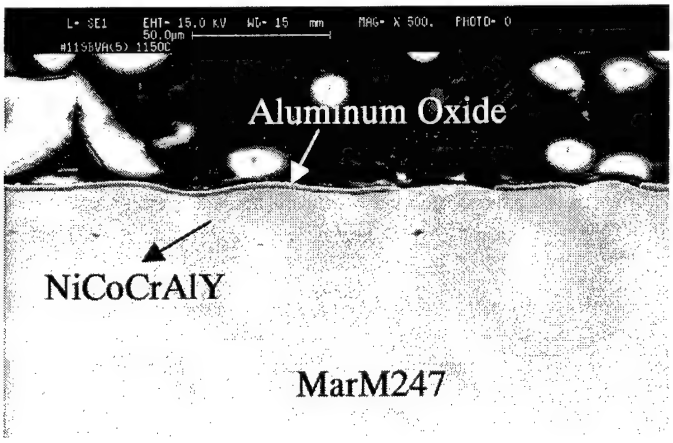

Figure 6. Surface rumpling of a NiCoCrAlY bond-coat for a sample exposed in air at 1150°C for 100 hours. Note how the oxide has spalled.

2.0 PHASE I APPROACH

UES, Inc.'s Phase I approach is illustrated in Figure 7. The most important component of the research was to develop a TBC system that comprised an alpha alumina sublayer, deposited by a novel filtered cathodic arc deposition system. The standard yttrium stabilized zirconia (YSZ) layer would be deposited on this sublayer by the electron-beam physical vapor deposition (EB PVD) technique. The rationale was that the high quality and fully stable alpha alumina layer would prevent oxidation of the metallic substrate. Discussions with the industry, both TBC manufacturers as well as engine companies, indicated that PVD was favored over CVD techniques, largely because the system could easily be integrated with EB PVD systems that are already in use for depositing YSZ.

The alumina layer was planned to be essentially defect-free, without the presence of mixed oxides that normally exist in thermally grown TGOs. The rationale was that this high quality alumina sublayer would be highly resistant to the inward diffusion of oxygen. Y doping would be considered because it has been shown to significantly reduce grain-boundary oxygen diffusion in alumina, the primary route for inward oxygen diffusion.

The technical work relied on a patented filtered cathodic arc deposition process [11,12] to deposit the alpha alumina sublayer at elevated temperatures (see Figure 8). This process provides high plasma ionization (>90%) compared to standard PVD processes (<20%). The multiply charged ions provide high reactivity of the plasma, thereby allowing very good bonding to the substrate. With high current densities (~ 4-5 A/cm^2) possible in the arc process, the percentage of neutral molecules can be reduced to less than 0.1%. The filtered arc source allows deposition of droplet-free coatings by deflecting the plasma flow along the curvilinear magnetic lines of force towards the substrate, while the droplets, having straight trajectories, are captured on the baffles. This advanced filter design provides practically droplet-free coating on large areas, ranging from about 250 mm in width to heights on the order of 300 mm. The patented auxiliary anode assembly facilitates the generation of a uniform, high density plasma in which the part is immersed. Consequently, the process is much less sensitive to line-of-sight issues, as is the problem with standard sputtering and EB PVD techniques. Also, the high degree of ionization, combined with the plasma blanketing effect, permits deposition of extremely uniform coatings without roughness or ridges.

The vacuum arc cathode is also a theoretically unlimited electron emitter, thus providing an efficient source of high-density electron current. In this mode, it facilitates the generation of a uniform, highly conductive ionized gas even without the metal plasma. This is utilized for ion-cleaning the substrate before coating deposition.

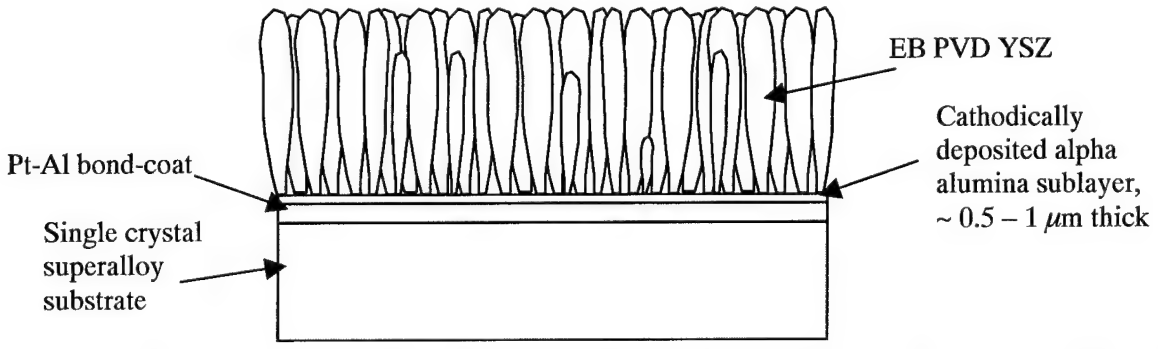

Figure 7. UES's approach for the TBC system. The coating consists of a Pt-Al bond-coat, followed by a 0.5 – 0.6 μm alumina sublayer deposited by the filtered cathodic arc technique. The thermal barrier YSZ layer (~100 μm thick) is deposited by EB PVD.

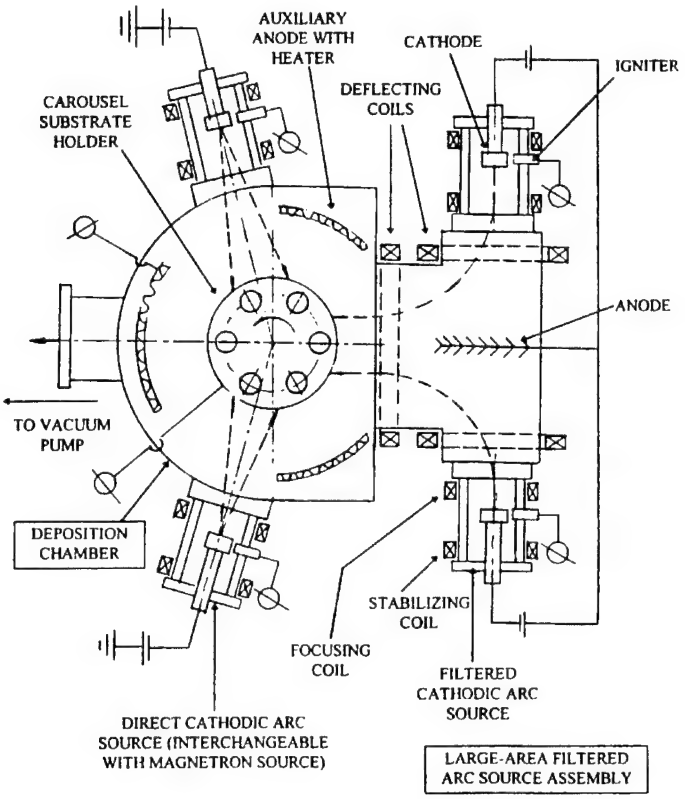

Figure 8. Sketch of the filtered cathodic arc deposition equipment at UES, Inc. showing the arrangements of the direct and filtered arc sources, auxiliary anode assembly, and substrate holder. The effective zone of deposition is approximately 15 inches in diameter and 16 inches high. The rotating carousal has 12 independent mounts and there are 4 layers.

3.0 RESEARCH TEAM

The research program involved a collaborative and consultative effort between the following industries and academic institutions:

(1) UES, Inc.: Prime contractor and coordinator. Preparation of samples, cathodic arc deposition of alumina coatings, AES analysis. PI: Rabi Bhattacharya.

(2) Rolls-Royce Allison: Engine partner for advice on coating architecture and performance, and supplier of the CMSX-4 superalloy that is used in their engine. PI: Dr. William Brindley

(3) Howmet Corporation: Casting of the single-crystal CMSX-4 alloy, Pt electroplating and aluminizing for the Pt-Al bond-coat, electron beam physical vapor deposition (EB PVD) of yttria stabilized zirconia (YSZ). PI: Dr. Ken Murphy

(4) New Mexico Tech: Thermal cycling of TBC coated samples between 200°C and 1150°C, and characterization of coating and microstructure before and after thermal cycling. PI: Dr. Bhaskar Majumdar

(5) Stevens Institute: Consultative discussions on TBC performance and TBC architecture. PI: Dr. Wu Lee.

4.0 EXPERIMENTAL PROCEDURES

The base material selected for the investigation was a single crystal CMSX-4 that is used in advanced turbine blades. This alloy has a very high volume fraction of cuboidal γ' phase ($L1_2$, approximately 60-65%, ~200 nm size) with narrow channels (~50 nm width) of continuous γ (disordered fcc) phase between the γ' phase. The cast rod (Mold 11, Job No. AT0062.07.01) was fabricated at Howmet and supplied to UES, where the rod was machined and ground into coupons of approximately 25.4 mm diameter and 3 mm thickness. These were then supplied to Howmet for depositing the platinum aluminide bond-coat. This was accomplished by electroplating Pt (~75 μm thick) and then conducting low activity CVD aluminizing. The surface morphology of the Pt-Al bond-coat was illustrated in Figure 5, and shows grain sizes of 30 to 100 μm, and grain boundary ridges of height in the range 2 to 5 μm. These samples were then supplied to UES for deposition of alumina using the cathodic arc deposition technique.

The presence of the grain boundary ridges presented a dilemma. On the one hand, surface waviness is known to be responsible for out-of-plane delamination stresses, and may need to be avoided. On the other hand, surface roughness could also serve to prevent large scale delamination from a micro-defect, by providing a tortuous path to the growth of the delamination crack under buckling load; the TGO is under high compressive stress (~3 GPa) at ambient temperature. In this case, surface ridges could be beneficial.

There was one additional issue as well. In our previous program, we had observed that seeding of a surface with sub-micron alpha alumina particles was conducive to the growth of alpha alumina by the cathodic arc technique. The case in point was a seeded Si single crystal, which showed that alpha alumina could be grown at a lower deposition temperature (~850°C), compared to at least 950°C without the seeding. Although the result was not conclusive and needed additional validation, nevertheless it suggested that the presence of alpha alumina seeds could be conducive to forming alpha alumina by CAPVD. Note that it is important to grow alpha alumina, otherwise a non-alpha alumina layer would transform to stable alpha-alumina during service at temperatures above 1100°C, and the resulting transformation stresses would crack the alumina layer. Second indirect information in this regard is the practice of grit blasting the Pt-Al bond-coat prior to deposition of YSZ by EB PVD. The grit blasting is conducted with alumina particles, and does little to alter the grain boundary ridge structure. It is also doubtful whether the grit blasting helps in better mechanical interlocking of the very thin alumina layer on the bond-coat (formed during aluminizing) to the top YSZ layer. A recent conference presentation, wherein Raman spectroscopy was conducted on bond-coated samples exposed for two hours at 1100°C, suggested that kappa and theta alumina were present on non-grit blasted samples, whereas alpha alumina was present on grit blasted samples. Together, such information suggested that a part of the experimental design should include effects of the surface preparation.

The experimental design is provided in Table 1.

Control samples included as-received Pt-Al, polished Pt-Al, and alumina-particle grit blasted Pt-Al. The thermal cycling response of these samples would be compared with similar coupons with the CAPVD alumina coating. All the samples were provided to Howmet for depositing the top YSZ coating using the EB PVD technique.

Table 1. Surface condition of TBC coated samples

Sample Number	Description
1	Polished Pt-Al
2	Polished Pt-Al
3	Polished Pt-Al + CAPVD Alumina, Run 366
4	Polished Pt-Al + CAPVD Alumina, Run 366
5	Polished Pt-Al + CAPVD Alumina, Run 368
6	Polished Pt-Al + CAPVD Alumina, Run 363
7	As-received Pt-Al, No polishing
8	As-received Pt-Al, No polishing
9	As-received Pt-Al, No polishing + CAPVD Alumina, Run 368
10	As-received Pt-Al, No polishing + CAPVD Alumina, Run 370
11	Grit blasted Pt-Al
12	Grit blasted Pt-Al
13	Grit blasted Pt-Al + CAPVD Alumina, Run 369
14	Grit blasted Pt-Al + CAPVD Alumina, Run 369

The cathodic arc deposition of alumina was conducted at UES using 1100 grade aluminum targets as the cathode. Prior to introducing into the chamber, the samples were either ground and polished and ultrasonically cleaned in acetone and reagent grade methyl alcohol, or simply cleaned and dried; the latter for the as-received or grit blasted Pt-Al coated samples. Grinding (to remove grain boundary ridges) was conducted with successive grits of SiC, and then polished with diamond and finally 0.3 μm alpha alumina.

The depositions were conducted at high temperatures, in order to obtain the stable alpha-alumina phase. Because the existing filtered cathodic arc unit had capability only up to 450°C, a special tubular furnace was constructed with capability up to 1075°C. The sample was mounted inside the furnace, which was held horizontal to allow the impingement of Al and O_2 ions. This necessarily limited the coating to only one face of the sample. However, this limitation was considered sufficient for the Phase I program; UES already has a design to deposit alumina on the entire surface of turbine blades at high temperatures. It is important to note that the 1075°C capability is unique to any physical vapor deposition system, since the maximum capability of most systems is only about 850°C.

Prior to deposition of the alumina coating, the substrate was arc cleaned at the desired temperature of approximately 1000°C to 1050°C. Next, a mixture of oxygen and argon gas (approximately in the ration 80:20) was introduced into the chamber. The carrier argon gas was needed to minimize oxidation of the Al cathode, and thereby minimize instability of the arc. The substrate was RF biased, since prior research suggested that RF biasing was conducive to both improved coating/substrate adhesion, as well as the formation of high temperature phases.

Coating thickness was limited to 0.5–0.6 microns. This value was based on two considerations: (i) having a low enough thickness to reduce spalling of the alumina layer, since a smaller volume would necessarily possess less elastic energy that might drive an interface crack, and (ii) having adequate level of thickness, to reduce oxygen penetration into the substrate and thereby reduce oxide growth. Results suggest that the thickness of 0.5 μm may not be adequate to prevent oxidation.

In addition to these samples, CAPVD coating was conducted on two additional sets of polished samples. In one case, the sample was repolished on a clean nylon cloth with 0.3 μm alpha alumina. The higher hardness of the nylon cloth (versus billiard cloth) was utilized, to the extent possible, to embed

submicron alpha alumina particles for seeding purpose. The polished sample was subsequently rinsed in distilled water and argon dried, and not ultrasonically cleaned, to retain the submicron alpha alumina particles. Optical observations indicated that this method was sufficient to retain the particles of approximately 0.05 area-fraction. Because the area fraction was maintained low, the distribution was reasonably uniform, i.e., clustering was minimal. The primary objective here was to confirm the seeding induced alpha alumina nucleation phenomenon that was observed in our previous investigation. In the second set of samples, the alumina was doped with yttria (Y_2O_3) to reduce either the inward diffusion of oxygen or the outward diffusion of Al, primarily through the grain boundaries of the alumina coating. In particular, reference [13] indicated that the grain boundary diffusivity of 300 ppm Y doped alumina was three orders of magnitude lower than one without the yttria. In our experiment, Y doping (~2 atomic percent) was accomplished by embedding Y particles in the aluminum cathode. Auger electron spectra confirmed that this method of CAPVD deposition was indeed able to embed yttria in the alumina coating. It is relevant to note here that these coating runs were conducted towards the end of the program, and did not leave enough time for YSZ deposition and evaluation of thermal cycling resistance. Hence, only microstructural details of these alumina coatings are provided in this report.

The microstructures of samples were evaluated by sectioning and optical and scanning electron microscopic techniques. Our past investigation had confirmed the presence of alpha alumina in the CAPVD coatings that were deposited at temperatures of 950°C and higher. However, significant levels of carbon were noted in the previous investigation. Steps were taken to reduce surface contamination, and the effectiveness was evaluated using auger electron spectroscopy.

The thermal cycling resistance of the TBC samples was evaluated using a thermal cycling apparatus that was specially built for this project. The furnace is constructed around inexpensive SiC heaters (~$18/piece) that operate on 110 Volts, and can reach temperatures of approximately 1400°C in less than 30 seconds. Figure 9 shows the schematic of the apparatus. The sample is introduced into the furnace through the bottom by means of a pneumatic cylinder, which is controlled by a solenoid actuated pneumatic valve. The up and down motion of the sample is synchronized with the power into the furnace, such that the heaters are activated when the sample is introduced, and are deactivated when the sample exits from the bottom. Forced cooling was not required since the furnace synchronization itself was able to provide the needed cooling rate.

Two types of heating cycles were used. In both cases, the heating program consisted of 5-minute heat to 1150°C, a hold at 1150°C for 45 minutes or 70 minutes, a cool down to RT in 0.5 minute, followed by a hold at RT for 9.5 minutes. Thermal lag resulted in a heating time of approximately 12 minutes. During the cool-down phase, the sample reached 170°C before it was reintroduced into the furnace and heated once again to 1150°C. Thus, the maximum and minimum temperatures of the samples were 1150°C and 170°C, respectively. The hold times, after the sample reached 1150°C, were at least 30 minutes and 60 minutes for the two types of cycles. We designate them as short and long cycles, respectively. Most of the cycling was conducted with the short (30 minute hold cycle).

The thermal cycling was always conducted with companion samples, i.e., TBC coated samples with and without the CAPVD alumina layer. This allowed a direct verification of the effect of the alumina layer on TBC integrity.

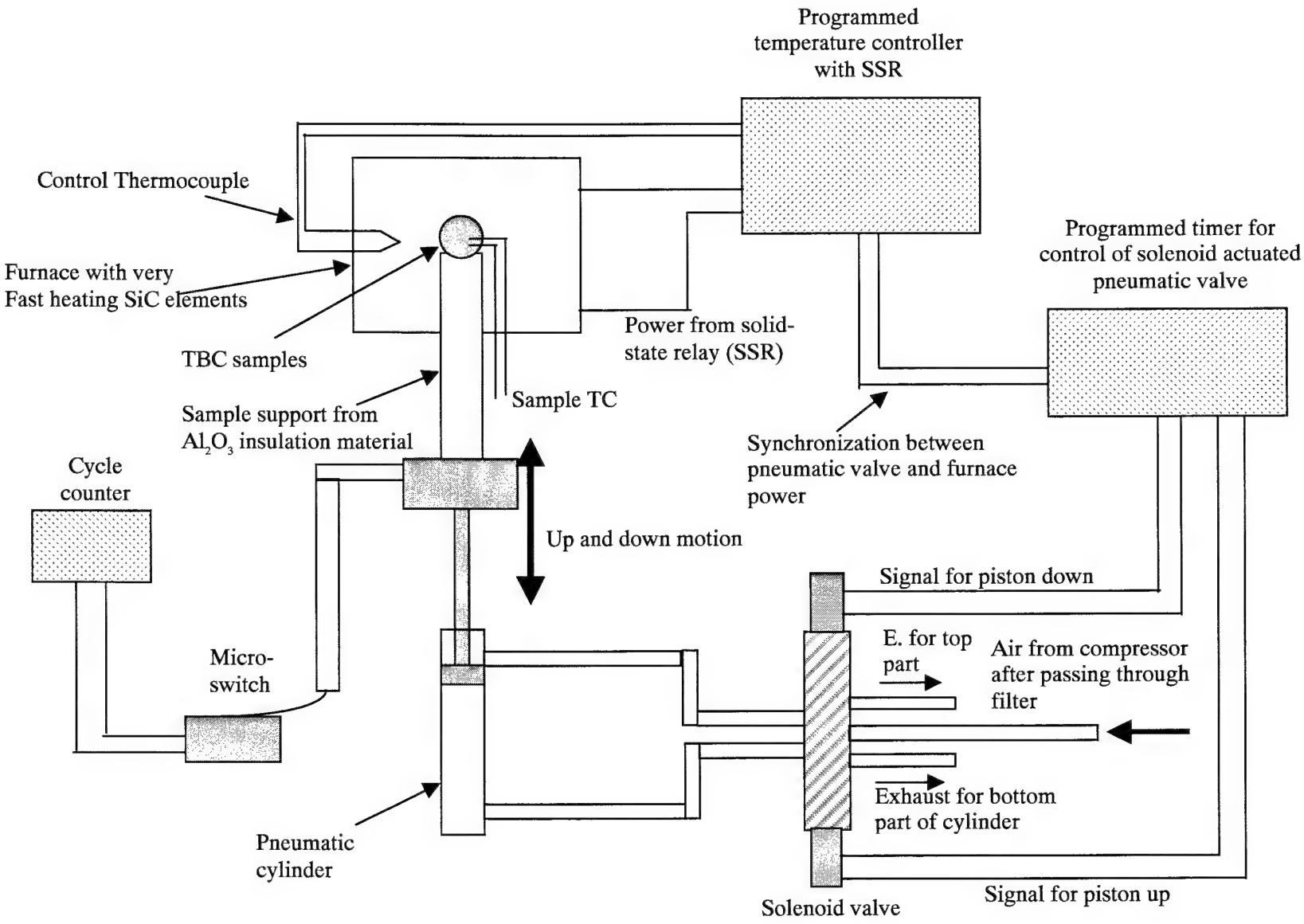

Figure 9. Schematic diagram of the thermal cycling apparatus.

5.0 PHASE I RESULTS

5.1 MICROSTRUCTURE

The surface morphology of the Pt-Al bond-coat was already illustrated in Figure 5. Figure 10 shows a cross-section of the microstructure of sample 6 that had already been subjected to 50 cycles between 170°C and 1150°C. In this micrograph, the single-phase β-(Ni,Pt)-Al layer extends to a depth of approximately 27 μm. Voids exist at this depth, and reaction induced particles/precipitates that are rich in refractory elements exist over an additional depth of approximately 30 μm from the void boundary.

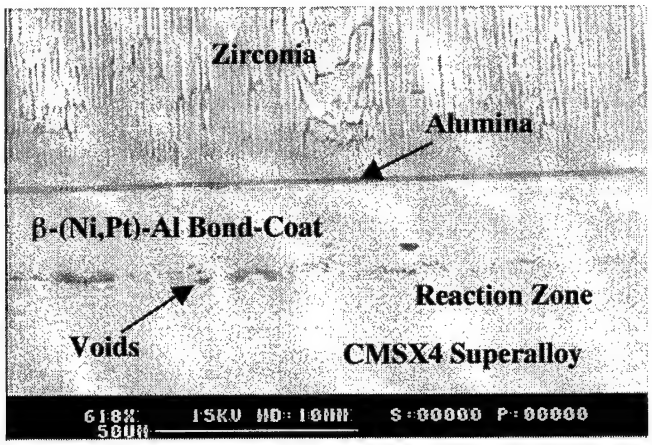

Figure 10. Cross-section of the microstructure of the Pt-Al coated CMSX-4.

Auger electron spectra (AES) of the alumina layer was analyzed to detect the presence of alpha alumina phase in the as-deposited CAPVD coating. In addition to the coated samples, both alpha and gamma alumina powder were evaluated. The results were analyzed using the "modified Auger parameter", α. This parameter is the sum of the Al-2p peak binding energy plus the Al KLL peak kinetic energy. The parameters for the different samples are provided in Table 2.

Table 2. Modified auger parameter for different grades of alumina and the CAPVD alumina coating

Sample	α (eV)
CAPVD Run 365+	1461.80
Buehler alpha alumina+	1461.92
Alpha alumina*	1462.09
Gamma alumina+	1461.55

\+ Measured in this investigation

* Data from Practical Surface Analysis, ed. D. Briggs and M.P. Seah, John Wiley & Sons, 1983, Appendix 4.

The measured value of α for alpha-alumina is 0.17 eV lower than the reported value for this phase (1462.09). Correcting for this difference, the value for the CAPVD alumina would be 1461.97 eV. This is very close to that for alpha alumina (1462.09 eV) than for gamma alumina (1461.55 eV). We conclude that the CAPVD phase is primarily alpha alumina. This result is also consistent with our previous investigation, where glancing angle X-ray diffraction and Raman scattering indicated the alumina layer to be primarily alpha alumina rather than gamma or kappa alumina.

Figure 11a shows the AES spectra of a CAPVD alumina coated sample, as a function of sputter time. The estimated sputter rate for Al_2O_3 is about 50Å/min. The spectra for alpha alumina is provided in Figure 11b for comparison. Together these figures show that the aluminum and oxygen concentrations are in the appropriate atomic ratio. In addition, carbon contamination is observed to be negligible, a problem that was faced in our previous investigation. Figure 12 shows the AES spectra for a sample that was coated with Y doped alumina. The spectra shows that the method of Y doping was indeed successful. Unfortunately, the sample was prepared quite late in the program, and prevented an investigation of the oxidation kinetics with the top YSZ layer.

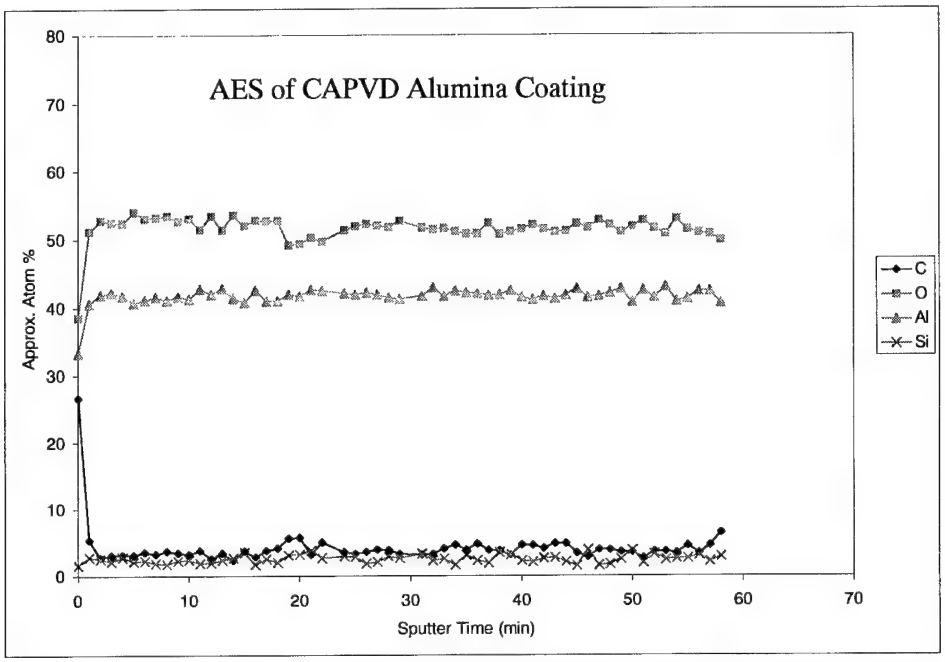

(a)

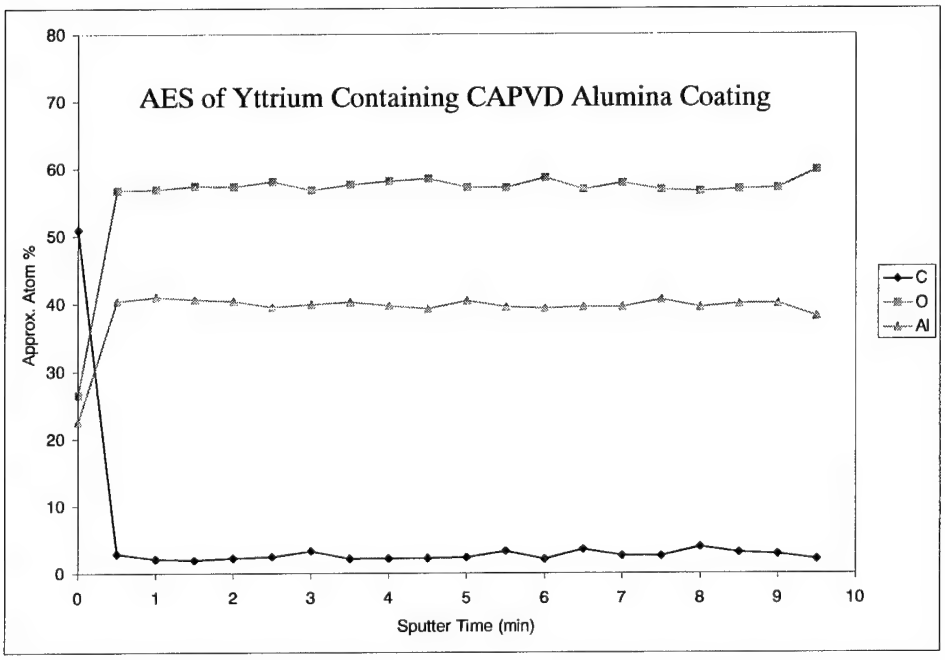

(b)

Figure 11. AES sputter profiles of (a) alumina coating deposited by cathodic arc and (b) sapphire (alpha-alumina).

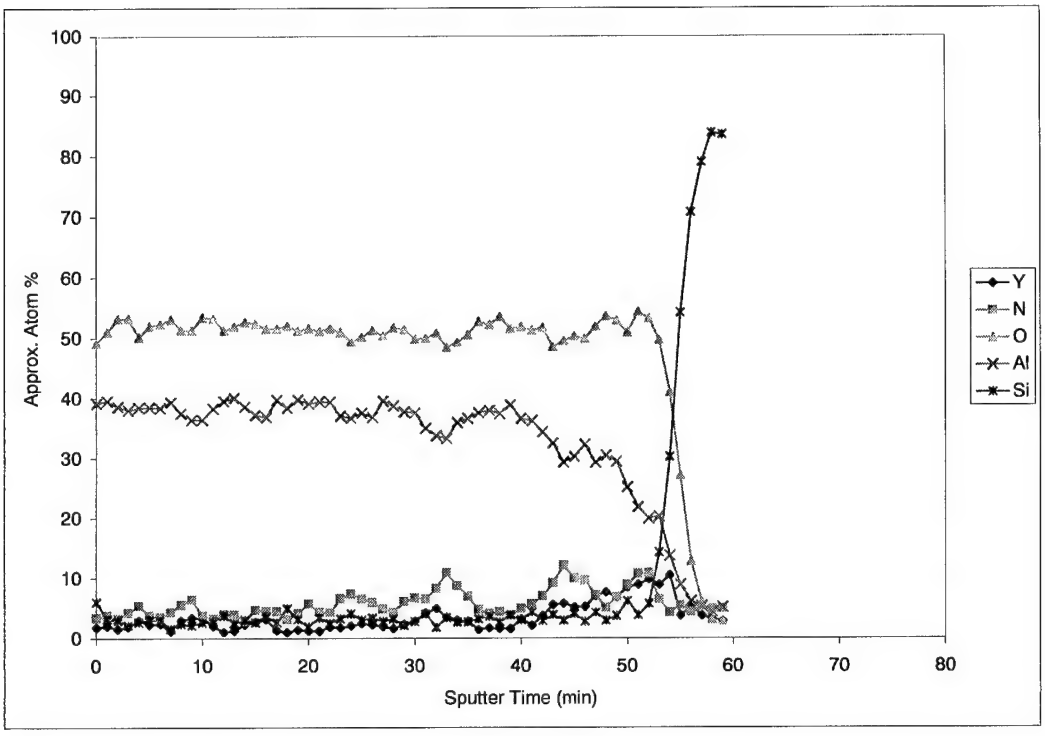

Figure 12. AES sputter profiles of a Y-doped alumina coating.

5.2 EVALUATION OF THERMALLY CYCLED SAMPLES

Figure 13 illustrates cross-section SEM of companion samples 1 and 6 that were thermally cycled using the short (30 minute) 170°C – 1150°C cycle, for 50 cycles. Both samples (see Table 1) were ground and polished to remove grain boundary ridges, prior to deposition of YSZ or alumina+YSZ. Sample 6 (with CAPVD alumina) showed slight delamination along the edges at the end of this 50 cycles, whereas sample 1 (without the CAPVD alumina) did not show any macroscopic delamination. Both samples were sectioned at the end of the 50 cycles. EDS analysis showed that the dark band between the top YSZ layer and the lower Pt-Al bond-coat was alumina. However, there appeared to exist subtle difference between the two samples. In the case of sample 1, the alumina layer appears to be fragmented and also gave the impression that there indeed existed a delamination crack, although the sample did not show any sign of delamination prior to sectioning. EDS of the dark band in Figure 13b also indicated alumina as the predominant phase, but there appears to exist a thin whitish line within the dark phase. The dark region next to the bond-coat is of the order of the thickness of the initial alumina coating (~0.5 μm), followed by a 1 μm thick alumina layer on top (next to the YSZ layer). This would suggest that there is outward diffusion of aluminum through the CAPVD alumina, followed by oxidation of those aluminum atoms. Our previous investigation also suggested this to be a possible mechanism of oxidation, but additional verification is still necessary.

The defects that were observed in samples 1 and 6 were quite small, but nevertheless suggest that the TBC coatings would have failed soon. Data in the literature suggest that advanced TBCs, consisting of a Pt-Al bond-coat and a highly compliant EBPVD YSZ, typically last more than 500 cycles when cycled between 200°C and 1150°C with a 30 minute hold time. Thus, our preliminary assessment from samples 1 and 6 is that grinding and polishing of samples prior to YSZ or alumina+YSZ deposition may not be good for TBC integrity.

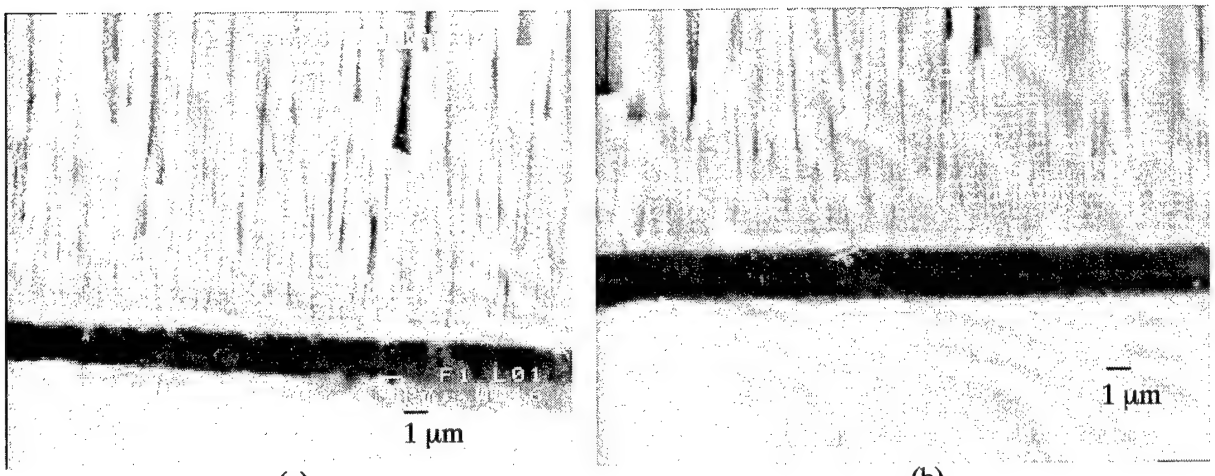

Figure 13. Cross-section SEM of (a) sample 1, without CAPVD coating and (b) sample 6, with CAPVD coating.

Figures 14a, b, and c are optical micrographs of samples 1 and 6. The alumina layer is indistinguishable at this magnification, but the damage provides some insight into the mechanism of delamination. Figure 14a is from sample 6 after it was thermally cycled, and although the circumferential edges were spalled, most of the TBC was intact. The alumina at the boundary between the YSZ and the bond-coat is located at approximately the whitish thin band that runs from left to right in the middle of Figure 14a. A few dark regions in the band may correspond to small delaminations, but the evidence is not conclusive. On the other hand, Figure 14b of sample 1 shows an elongated dark region where the alumina layer may have detached from the metal substrate. Figure 14c is a lower magnification micrograph from the same region as Figure 14b, and in this case the detachment regions are more obvious. What appears to be occurring is a non-uniform lowering of the metal layer on oxidation, but this is not accompanied with a simultaneous lowering of the YSZ layer. The result is the formation of isolated debonded regions. This is similar to the mechanism proposed in [14], wherein it was suggested that oxidation led to diffusion of Al and Ni to the metal surface.

In contrast to the ground and polished samples, the results from the grit blasted samples are extremely encouraging. Both samples 11 (without CAPVD alumina) and 13 (with CAPVD alumina) survived 920 cycles (with 30 minute hold at 1150°C) without delamination. Because of the long time spent on the test (almost 1.25 months), a decision was made to proceed to the long duration cycle time (60 min at 1150°C). The rationale was that if oxidation was primarily responsible for debond initiation, then a longer cycle time would accelerate the damage, because less time would be spent in cooling and reheating of the sample. After an additional 70 cycles with the 60-minute hold period, slight changes were observed between the two samples. Sample 11 indicated a small (1 mm size) ear near the edge of the sample, that could correspond to the start of delamination. On the other hand, sample 13 showed no signs of delamination whatsoever. At this point, the test temperature was raised to 1200°C. After 58 cycles at this temperature, both samples showed almost complete delamination of the TBC coating. Unfortunately, this behavior defeated our attempt to differentiate between samples with and without the CAPVD alumina layer. In retrospect, it appears that this temperature was too high for survival of the coating. Our preliminary observation suggests that the YSZ may have sintered at this temperature, and this may have largely been responsible for delamination in both the samples.

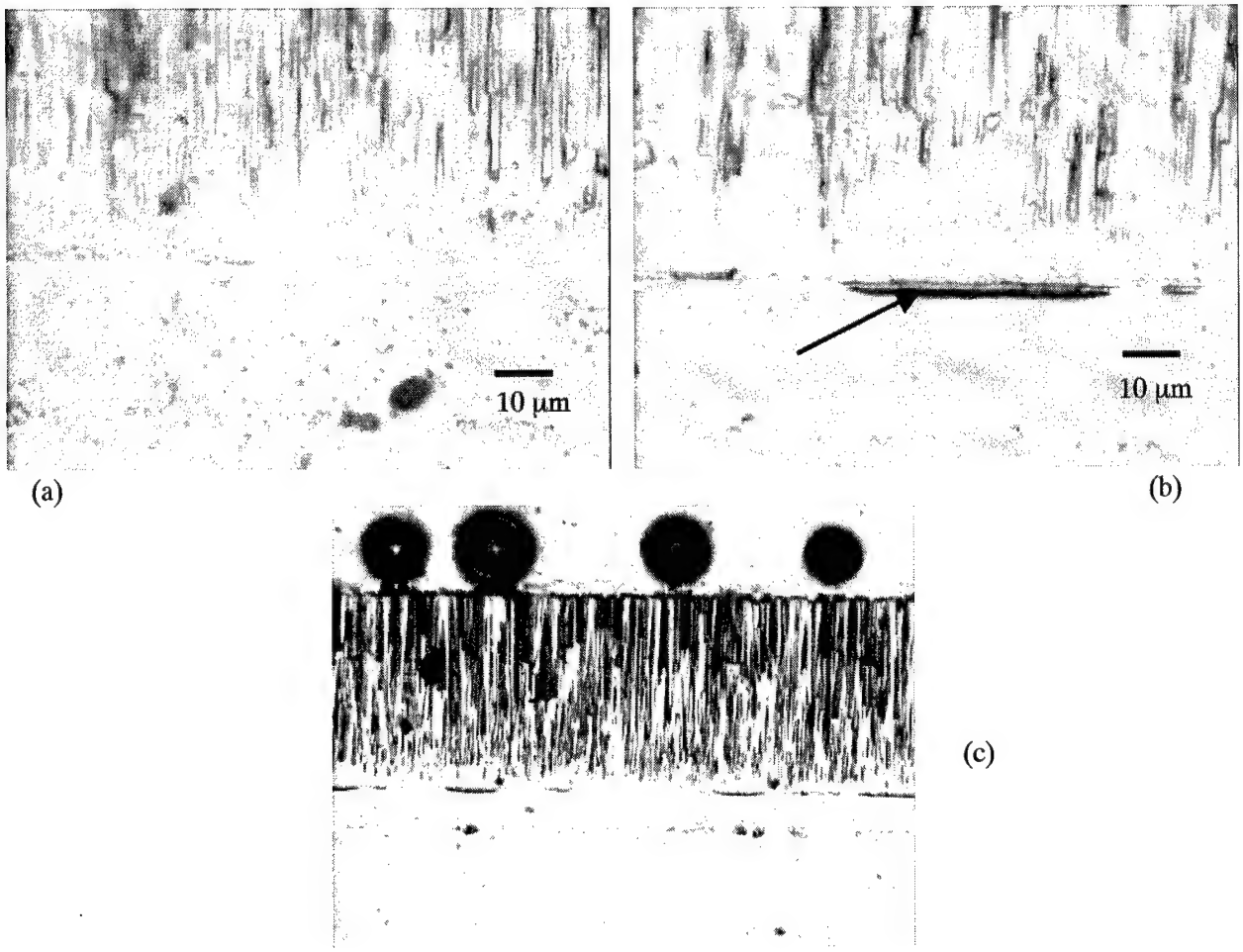

Figure 14. (a) Optical micrograph of polished sample 6 (with CAPVD) after thermal cycling. (b) Optical micrograph of polished sample 1 (without CAPVD) after thermal cycling. (c) Lower magnification optical micrograph of sample 1.

The fracture surfaces of samples 11 and 13 provide important distinction between the two samples. The stereo optical image in Figure 15 shows one edge of sample #11, where an ear had been observed on the TBC before the start of the 1200°C/1 hour-hold cycles (58 in all). The latter is sketched in the insert of Figure 15, and the location of the dark region in Figure 15 corresponds closely with the observed size and location of the YSZ before the start of the 1200°C exposure. Presumably this region had delaminated during the 1150°C cycles, and the subsequent thermal cycles up to 1200°C had significantly oxidized the region. As further evidence of this mechanism, the surface rumples on the bond-coat in this semicircular region may be compared with the morphology of the Pt-Al surface (the back surface) that had not been coated with YSZ (Figure 16). Both surfaces reveal a highly rumpled morphology, with a length scale that is about two to three times larger than the grain size, which is different from the grain morphology observed on the freshly delaminated surface after the 1200°C exposure (Figure 17). In contrast to sample #11, the CAPVD alumina coated sample (#13), did not reveal any delamination defect before the start of the 1200°C cycles. Thus, although both TBC samples exhibited delamination after the 1200°C exposure, sample 11 clearly shows evidence of greater damage than sample 13 during the regular 170°C – 1150°C cycles.

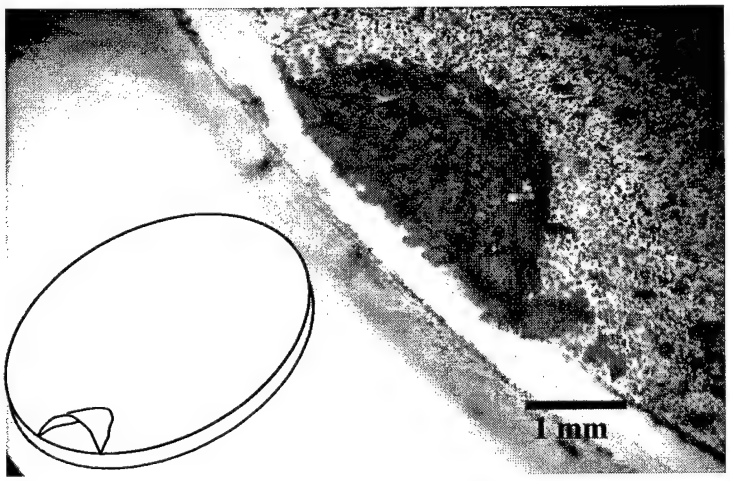

Figure 15. An oxidized region (dark semicircular shape) at one edge of sample 11 (without CAPVD), after the TBC delaminated following the 1200°C cycles. The inset sketch illustrates the observed shape of the small TBC delamination region before the start of the 1200°C cycles.

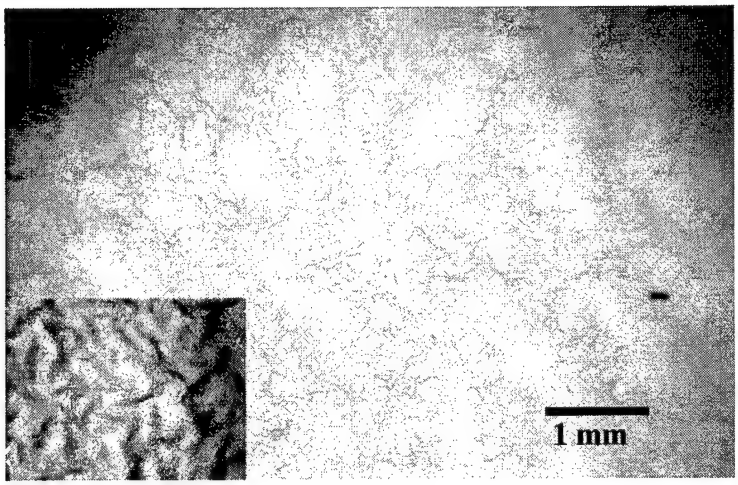

Figure 16. Morphology of Pt-Al bond-coat surface on the back face; i.e., the face not coated with alumina or YSZ. The inset at the bottom left illustrates the wrinkled but strongly adhering oxide layer on the Pt-Al surface at a higher magnification.

Figures 17a and 17b are low magnification optical stereo images of samples 11 (without CAPVD) and 13 (with CAPVD), respectively. Both figures reveal the original grain structure of the Pt-Al bond-coat. The bright and shiny regions (spots, lines, and areas) correspond to locations where the bond-coat metal is exposed. This was concluded based on the natural shiny color of metallic surfaces[2], and from lack of oxygen assessed from EDS analysis when observed in the SEM. In contrast, the dark and dull whitish regions in Figure 17 correspond to oxidized material, and the EDS spectra showed the predominant elements to be aluminum, and oxygen. Our preliminary assessment is that the shiny surfaces

[2] A case in point was the oxidized back surface of the samples, which were dark in color, but without oxidation pits that are normally observed in oxidized NiCoCrAlY bond-coats. Rather the back surface showed wrinkles of the oxidized material, and although the wrinkles had size scales similar to Figure 5b, they were distorted from the initial grain boundary ridge pattern on the Pt-Al bond-coat.

(a) Without CAPVD

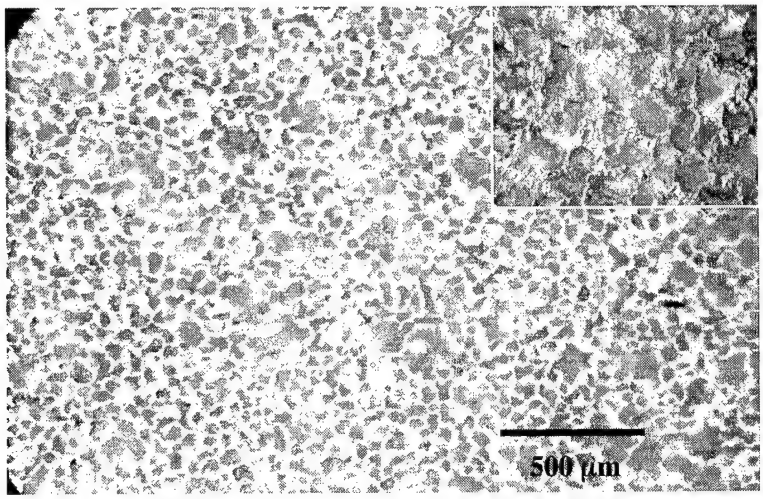

(b) With CAPVD

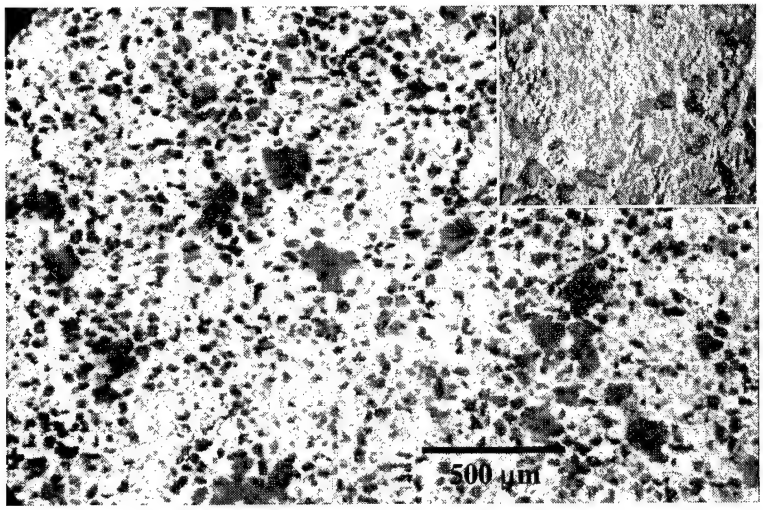

Figure 17. (a) Morphology of the bond-coat surface of sample 11 (no CAPVD) after the YSZ had delaminated following the 1200°C cycles. (b) Corresponding morphology of sample 13 (with CAPVD alumina) after TBC delamination. Higher magnification of these optical micrographs are provided in the inset at the top right of each picture. The fracture surface reveals the bond-coat grain morphology. Note the difference in area occupied by the white regions in the two micrographs. The white/bright regions revealed negligible oxygen, and suggest failure at the metallic bond-coat surface. The dark regions revealed significant oxygen and Al levels, and suggest failure at the TGO/YSZ interface.

came about during fast delamination of the entire TBC at the end of TBC life, whereas the dull/dark texture was a result of accumulated oxidation damage during prolonged exposure of the bond-coat at temperature. In this case, it appears that the TGO may have separated from the YSZ during thermal cycling by a mechanism of non-uniform cave-in of the bond-coat, and this was followed by even greater oxidation of the bond-coat. Consequently, when the TBC finally failed, possibly during a cool down phase from 1200°C, these locations remained attached to the metal. Figure 17a shows that the predominant texture of sample 11 was dull/dark with the shiny metallic regions only at the grain boundary (of the Pt-Al) locations. On the other hand, Figure 17b shows greater area coverage of the shiny metallic regions than Figure 17a, with the shiny regions often spanning many grains. The insets on the top-right corner of the micrographs illustrate these features at a higher magnification. If our

interpretation of the shiny and dark morphologies are correct, then the differences in morphology of the two samples suggest that more damage may have accumulated in sample #11 than in #13 during the regular 170°C to 1150°C thermal cycling. The sintering of the YSZ due to 1200°C exposure may have largely contributed to buckling induced failure, and limited our ability to determine which sample would have lasted longer with the standard cycling procedures.

Figures 18a and 18b are cross section SEM of samples 11 and 13, respectively. YSZ is not visible in either micrograph since the TBC had completely delaminated, except for some small regions near the edges. In Figure 18, the waviness of the bond-coat surface/TGO interface of sample 11 may be compared with the less wavy surface of sample 13. Also, the TGO alumina is adhering to the bond-coat in Figure 18a, and its grainy texture may be observed on the upper side of the alumina. Essentially, the top plastic region of the epoxy mount had rounded off during polishing, thereby revealing the texture of the TGO alumina towards the YSZ face; i.e., we are observing a three-dimensional feature of the TGO. In contrast, Figure 18b (sample 13) shows that the metal surface is completely exposed, consistent with the shiny metallic fracture surface morphology discussed in the previous paragraph. Further evidence of this failure morphology is revealed in Figure 19, which shows part of the YSZ that had delaminated from the bond-coat in sample 13. The bottom band attached to the YSZ is purely alumina, as determined from EDS spectra. Thus, whereas much of the damage occurred at the alumina-YSZ interface in sample 11, it occurred at the alumina-metal surface in sample 13. Our assessment is that the former occurred during the 1150°C thermal cycles, so that sample 11 would likely have had TBC failure even without a temperature increase to 1200°C. On the other hand, the damage during thermal exposure was much less in sample 13, so that this sample may have exhibited improved cyclic life if the YSZ had not partially sintered through a 1200°C exposure. It is also of interest to note the thickness of the alumina in the two samples. In sample 11 the TGO layer is approximately 6–7 μm thick, whereas in sample 13 it was only about 3–4 μm thick. Thus, the CAPVD alumina was able to reduce oxidation of the bond-coat, which in turn resulted into reduced damage of the TBC.

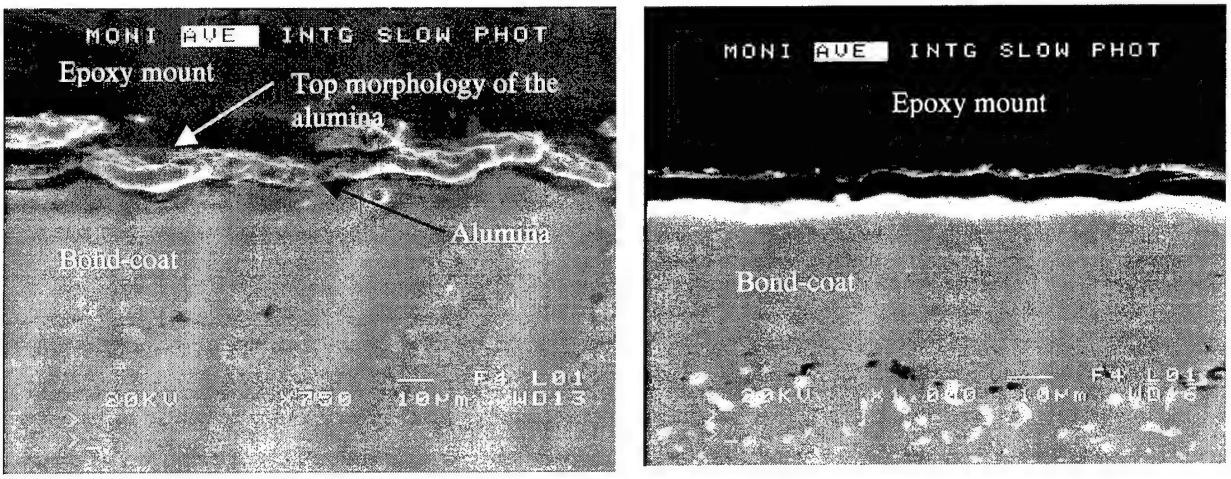

(a) Without CAPVD (b) With CAPVD

Figure 18. (a) Cross-sectional SEM of sample 11 after TBC delamination. (b) Corresponding micrograph of sample 13.

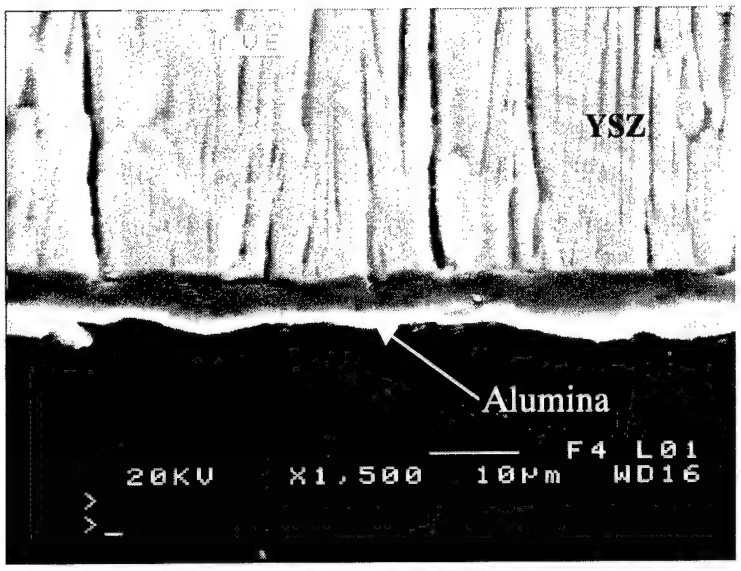

Figure 19. Cross-sectional SEM of sample 13 (with CAPVD alumina). Here, the YSZ has delaminated from the bond-coat, and all the alumina is sticking to the YSZ.

6.0 DISCUSSION

An alumina sublayer architecture was utilized in this program to improve the thermal cycling life of an advanced TBC system. The rationale was that a high quality alpha alumina layer would significantly reduce or eliminate oxidation of the bond-coat, a prerequisite for delamination of the TBC. The system consisted of a CMSX-4 single-crystal superalloy substrate with a (Ni,Pt)-Al bond-coat, a layer of alumina (approximately 0.5 μm thick) deposited by the cathodic arc physical vapor deposition (CAPVD) technique, and a subsequent yttria stabilized zirconia (YSZ) layer of 70 μm thickness deposited by the electron beam physical vapor deposition (EB PVD) technique. The effect of the alumina layer was determined by comparing the thermal cycling response of TBC samples with and without the CAPVD alumina layer.

The integrity of the alumina sublayer is affected by its stability, and so CAPVD was conducted at temperatures around 1000°C to obtain the alpha alumina phase. The presence of this phase was determined by Auger electron spectroscopy (AES) and by comparing the modified binding energy parameter with those of alpha and gamma phase powders. The results indicate alpha phase as the primary phase in the CAPVD alumina, and was consistent with similar results obtained previously using glancing angle X-ray and Raman spectroscopy techniques. CAPVD was also utilized to deposit alumina doped with yttria. The rationale was based on available data in the literature, which suggested that the presence of yttria at the grain boundaries of alumina could substantially reduce diffusion of Al^{3+} and O^{2-}. In fact, a few orders of magnitude drop in the parabolic oxidation rate constant (k, in x^2 =k.time), from the current value of about 10^{-13} cm^2/sec at 1150°C, could be realized through such a doping technique. AES profile on a yttria doped substrate confirmed the success of the CAPVD technique, but lack of time prevented thermal characterization of this alumina layer.

The effect of surface preparation prior to alumina deposition was evaluated by considering: (i) ground and polished bond-coat surface, (ii) as-received bond-coat surface, and (iii) a bond-coat surface grit blasted with alpha alumina. The latter technique is often used in the industry, although the scientific merit and principles have not yet been thoroughly investigated. In this program, grit blasting was

considered because a prior research by the current investigators suggested that alpha alumina seeds could enhance formation of alpha alumina during CAPVD deposition.

A robust thermal cycling apparatus was fabricated to allow thermal cycling of samples at temperatures up to 1200°C. Most of the thermal cycling tests consisted of cycling between 170°C and 1150°C with a hold time of about half hour at 1150°C. Because valuable time was lost at the start of the program in acquiring the CMSX-4 single crystal, and because of the long cycle times, only limited experiments could be completed on the TBC samples. The results are not conclusive, but nevertheless provide important insight on the mechanisms of TBC spallation, and the effectiveness of the alumina sublayer in extending TBC life.

Tests with ground and polished samples indicate that removal of the grain-boundary-ridged morphology of the bond-coat is not conducive to TBC integrity. It appears that any defect in the alumina coating could enhance propagation of damage, since a potential delamination crack could grow without barriers imposed by the presence of grain boundary ridges in the bond-coat.

The most encouraging results were obtained with the grit blasted samples. Following an initial survival of about 1000 cycles, the companion samples (with and without CAPVD alumina) were subjected to one hour exposure at 1150°C. After approximately 70 cycles under this condition, a small lift off of the YSZ was observed in one corner of the control grit blasted sample, but not in the CAPVD sample. At this point, the maximum temperature was raised to 1200°C, and unfortunately both TBCs were found to have spalled when they were inspected after 58 cycles at this temperature. The YSZ layer suggested sintering of the columnar YSZ grains, and this may have precipitated rapid damage and ultimate delamination.

The morphology of the fracture surface, as well as sectioning of the delaminated samples, suggest that damage at the bond-coat interface occurs by a surface rumpling mechanism that is limited by the size of the (Ni,Pt)-Al grains. The bond-coat surface that was not coated with YSZ also revealed surface rumpling but of size scale two to three grain diameters. More significantly, the wrinkling and surface features of this YSZ-free face pointed to an extremely tenacious oxide. In contrast, while NiCoCrAlY bond-coats do form oxide layers, we have observed them to repeatedly spall and give rise to a pitted surface. Clearly, the Pt-Al bond-coat is preferable in any high performance oxidation application.

While both grit blasted samples (#11 and 13) exhibited delamination under the severe 1200°C thermal cycling conditions, the delaminated bond-coat surface provided useful insight. The grain boundaries showed a shiny-ridged morphology, and EDS measurements indicated the absence of any significant level of oxygen at those shiny locations. Our initial conclusion is that those locations with metallic luster correspond to freshly exposed bond-coat surface, and that this likely happened during the last few thermal cycles. The grain interiors were darker, and EDS revealed that those areas were essentially pure alumina, with traces of YSZ in isolated locations. Here, our initial conclusion is that these regions had already delaminated from the YSZ layer, so that when final fracture occurred, those regions remained attached to the bond-coat.

Figure 20 illustrates the possible sequence of damage. Oxidation of the bond-coat is accompanied by a flux of primarily Al and some Ni atoms to the surface. This flux alters the internal microstructure, including increase in grain size and changes in the volume fraction of different phases (both observed previously in a NiCoCrAlY bond-coat), at distances up to 50 μm from the TGO interface. Such changes can cause shrinkage of the bond-coat, as we have suggested in our previous study and also suggested recently by Tolpygo and Clarke. [14]. Since the bond-coat is attached to the substrate (iso-strain), shrinkage can only take place in the thickness direction. The shrinkage maybe non-uniform due to different diffusion rates near the bond-coat grain boundaries, and also from other microstructural non-

uniformity inside the bond-coat and bond-coat/superalloy reaction zone. The observed morphology of the fracture (delaminated) surfaces suggests a metal contraction illustrated in Figures 20b and 20c, wherein the grain boundary ridges remain fixed, but the grain interiors contract downward. The bending stiffness of the YSZ layer, largely because of its thickness (~70 μm), prevents a conformal deepening of the YSZ inside the valleys. The result is delamination of the alumina layer from the YSZ. When final TBC failure occurs, such delaminated regions remain attached to the bond-coat, and YSZ failure occurs at the ridges. The metallic character at the ridge locations suggest that the delamination cracks find their way through the oxide layer at the ridges, and essentially graze the metallic surface. We note that creep of the bond-coat may be one additional factor that enhances surface rumpling, but this effect should be similar for both un-oxidized and oxidized samples.

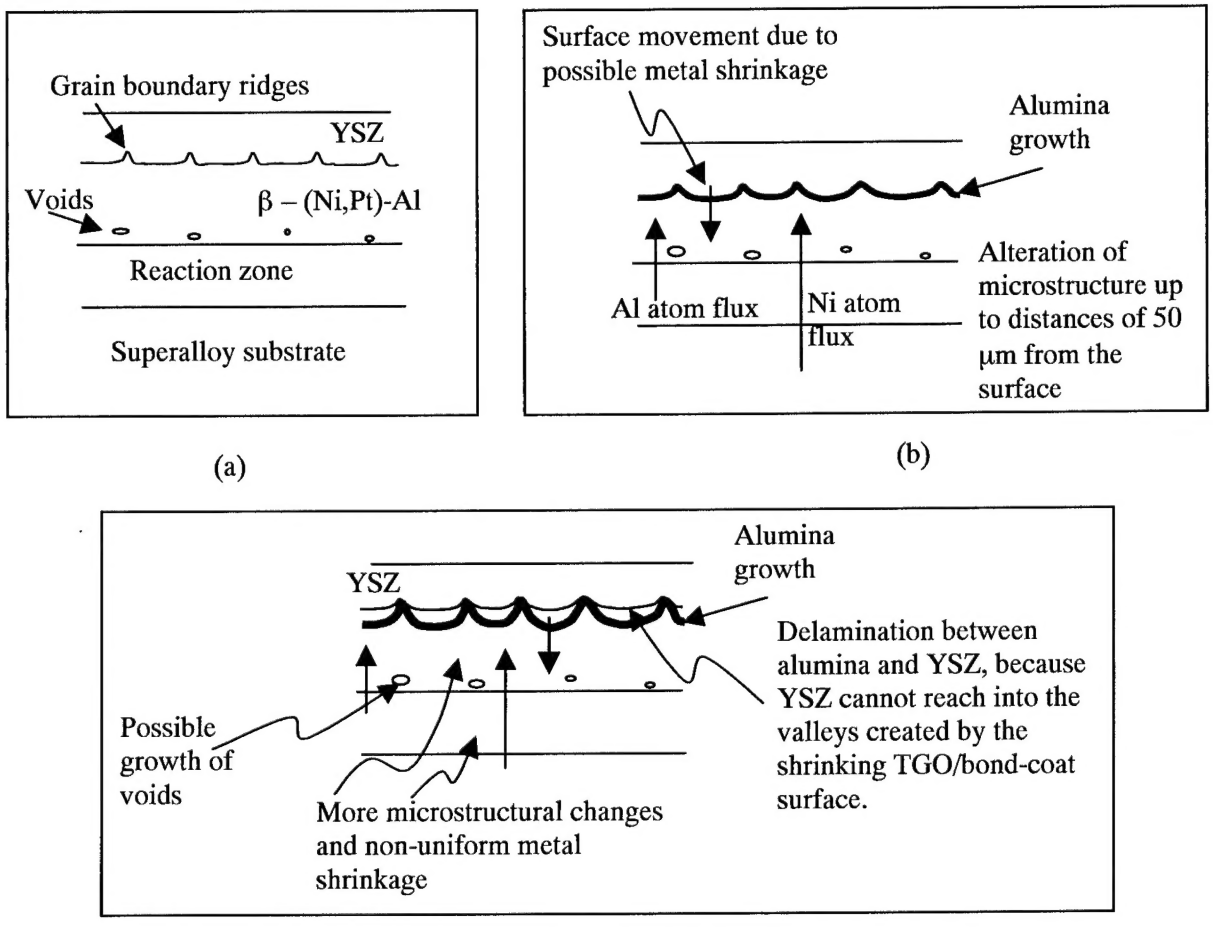

Figure 20. Schematic illustration of the nucleation and progression of damage.

In this scenario of failure, the extent of oxidation damage can be assessed from the fraction of alumina sticking to the bond-coat surface. If the oxide regions are large and occupy almost completely the grain interior, as was observed for the control sample, then significant oxidation can be interpreted. Note that greater oxidation (TGO growth) of the bond-coat is accompanied with greater flux of Al and Ni atoms from the interior and consequently more microstructural changes. This will result in more metal shrinkage, and hence greater area of delamination between the TGO and the YSZ. On the other hand, if the metallic regions are larger, then one may interpret smaller shrinkage and surface rumpling, as well as

less oxidation of the bond-coat. The TBC sample with the CAPVD alumina layer revealed this type of behavior. The fracture surface morphology was also consistent with less rumpled morphology of the bond-coat surface, when observed on a transverse section. In addition, while a small delamination was observed on the control sample prior to the 1200°C cycles, none was observed for the CAPVD sample. Thus, although both samples were found to be delaminated after the 58 cycles at 1200°C, the CAPVD sample appears to have performed better in terms of preventing oxidation and rumpling of the surface.

We reiterate that the results are not conclusive. Nevertheless, the grit blasted CAPVD sample appears to have performed better than the control grit blasted sample. Further tests, where samples are thermally cycled to failure between 170°C and 1150°C, are needed to confirm the current findings. Indeed, one additional set of samples has been cycled for 100 cycles, and they will be provided to Rolls Royce for thermal cycling evaluation. It is also important to note that while there had been concerns regarding the bonding of the CAPVD alumina to both the YSZ and the bond-coat, the current results indicate that indeed good bonds may be obtained between the layers. Finally, the metallurgical observations provide insight into the mechanisms of TBC damage. The significant difference from previous models of TBC damage is that the mechanism of damage growth appears to be one of surface rumpling, rather than TGO delamination by local buckling.

7.0 CONCLUSIONS

The following conclusions may be derived from this work:

1. The cathodic arc deposition technique can be conveniently utilized to deposit alpha alumina layer on advanced (Ni,Pt)-Al bond-coat.
2. Excellent TBC life is obtained when alumina is CAPVD deposited on as prepared Pt-Al bond-coat, grit-blasted with alumina.
3. Comparison of thermally cycled companion TBC samples showed less oxidation damage of the CAPVD alumina-containing sample than the control grit blasted sample.
4. The mechanism of TBC damage initiation and growth appears to be one of surface rumpling caused by non-uniform metal shrinkage.

REFERENCES

1. T.E. Strangman,"Thermal Barrier Coatings for Airfoils," Thin Solid Films, 127, p. 93-105 (1985).
2. J.T. Demasi et al., "TBC Life Prediction Model Development," P&W, NASA C.R.-182230 (1989).
3. J.T. DeMasi-Marcin and D.K. Gupta, "Protective Coatings in the Gas Turbine Engine," Surface Coat. Tech., *68/69,* 1 (1994).
4. J. Doychak, J.L. Smialak, and T.E. Mitchell, "Transient Oxidation of Single Crystal Beta NiAl," Metall. Trans., 20A, p. 499 (1989).
5. R. Prescott, D.F. Mitchell, M.J. Graham, and J. Doychak, Corrosion Sc., Vol. 37, p. 1341 (1995).
6. I.G. Wright, B.A. Pint, W.Y. Lee, K.B. Alexander, and K. Prusner, Proceedings of Institute of Materials Conference on Surface Engineering, Edinburgh, UK (1997).
7. V. Sergo, X. Wang, D. Clarke, and P.F. Becher, J. Am. Cer. Soc., 78, 2213 (1995).
8. J.A. Ahmad et al., "Design Tool for Oxidation and Thermal Protection Coatings," USAATCOM TR 96-D-11, Final Report to US Army Aviation Command, Oct. (1996).
9. W.Y. Lee, D.P. Stinton, C.C. Berndt, F. Erdogan, Y.D. Lee, and Z. Mustasin, "Concept of Functionally Graded Materials for Advanced Thermal Barrier Coating Applications," J. Am. Cer. Soc., Vol. 79, No. 12, p. 3003-3012 (1996).
10. "Advanced Thermal Barrier Coating", DoD SBIR Phase I Final Report, Contract No. F33615-99-C-5206, April 21, 1000.
11. V.I. Gorokhovsky, U.S. Patents No. 5,380,421 and 5,435,900 (1995).
12. V.I. Gorokhovsky, Surface and Coatings Technology, Vol. 61, 108 (1993).
13. M. Le Gall, A.M. Huntz, B. Lesage, C. Monty, and J. Bernardini, "Self-Diffusion in Alpha Alumina and Growth Rate of Alumina Scales Formed by Oxidation: Effects of Yttria Doping," J. Mat. Sci., p. 201-211 (1995).
14. V.K. Tolpygo and D.R. Clarke, "Surface rumpling of a (Ni,Pt) bond-coat induced by cyclic oxidation", Acta Metall. Mater., Vol.48, p 3283-3293 (2000).